Biomass Conversion and Biorefinery (2023) 13:15565–15576
https://doi.org/10.1007/s13399-022-03009-8

ORIGINAL ARTICLE

Biochar derived from mild temperature carbonization of alkali-treated sugarcane bagasse for efficient adsorption to organic and metallic pollutants in water

Chunxiao Yang[1] · Haoyi Wu[2] · Xianzhi Zeng[2] · Zhongshuo Pan[3] · Huidan Tan[3] · Shan Chen[3]

Received: 10 April 2022 / Revised: 19 June 2022 / Accepted: 27 June 2022 / Published online: 8 July 2022

Abstract

Persistent organic pollutants (POPs) and metals are harmful pollutants; thus, their emission and diffusion need to be controlled. Biochar derived from biomass shows potential application in pollutant adsorption. Sugarcane bagasse raw (SCR) is a major by-product of the sugar industry, and its added value will be well exploited by a proper carbonization process with a mild temperature. In this work, biochar samples were prepared using simple and cost-effective carbonization to the SCR at 300 and 400 °C (roughly corresponding to the complete volatilization of hemicellulose and cellulose, respectively). The alkali (NaOH) pretreatment was employed, and their activation process was investigated at these temperatures. It was found that alkali pretreatment resulted in significant changes in specific surface area (SSA) and total pore volume (TPV) significantly as compared to those without alkali activation. The changes in surface morphology and oxygen-containing functional groups (mainly C–OH) were observed, especially on the activated one at 400 °C, where the samples showed a pore structure and cracks with uneven distribution. Thus, RhB and Cr(III) which were selected as the represented contaminants were efficiently adsorbed by the samples with alkali pretreatment. Moreover, an excellent monolayer coverage adsorption per unit specific surface area (0.82–57.79 mg/m^2) was observed. The adsorption process of RhB on alkali-biochar could be dominated by physisorption, while chemisorption was for Cr(III). In addition, competitive adsorption behavior was speculated to exist between the sodium oxide embedded in alkali-pretreated biochar and Cr (III) in the aqueous phase. Therefore, with a simple alkali pretreatment and a mild temperature carbonization, SCR could be transferred to biochar with adsorption to both POPs and metal ions. This method will be suitable to mass production of biochar for environmental protecting application.

Keywords Pyrolysis · NaOH activation · Adsorbent · Removal mechanism

1 Introduction

Persistent organic pollutants (POPs) and metals are the harmful pollutants because they are bioaccumulated up the food chain and cause adverse problems in the human body, i.e., carcinogenic and mutagenic [1–3]. They are generally produced in industries such as paper making, dyeing, closing, and electroplating, diffused with the wastewater, and are difficult to totally remove from sewage [4–6]. For the purpose of environmental protection and sustainable development, controlling their emission and diffusion is becoming a critical issue. By now, many methods have been developed for advanced water treatment to remove POPs and metal ions, including physical adsorption [4, 7], membrane separation [2], chemical and biological reactions [6], and catalysis [8–10]. Among these methods, physical adsorption is a suitable one for its efficient treatment and cost-effectiveness [1, 4]. Therefore, exploring the advanced adsorbents for the efficient adsorption of POPs and metal ions remains a challenging concern. Compared to mesoporous silica [11], zeolite [12], or metal–organic framework [13], biochar derived from biomass, i.e., sugarcane [14], pinecone [15], and wheat husks [9], shows more competitiveness because

✉ Haoyi Wu
manofchina@outlook.com

[1] School of Analysis and Test Center, Guangdong University of Technology, Guangzhou 510006, China

[2] School of Physics and Optoelectronic Engineering, Guangdong University of Technology, Guangzhou 510006, China

[3] School of Environmental Science and Engineering, Guangdong University of Technology, Guangzhou 510006, China

of the abundance in the earth, easy preparation and low cost, which allow their mass production for scalable application in industry.

Sugarcane residue is one of the by-products generated in a large quantity in the sugar industry [16]. For instance, millions of tons of sugarcane bagasse is produced in China, Brazil, and India on a wet basis annually [17–19], and a considerable quantity of this residue is used as boiler fuel, since its added value has not been properly exploited [20, 21]. Since sugarcane is rich in fibrous lignocelluloses, its residues are chemically composed of cellulose, hemicellulose, and lignin, which are highly carbon-containing [16, 22]. Noncovalent forces and covalent cross-linkages connect these components, providing strength to the plant cell wall and forming a complex network [23]. Therefore, sugarcane bagasse can serve as a potential biomass for the conversion to biochar with a complex network that may induce a porous structure and possibly apply in physical adsorption to POPs and metal ions in water [24–26].

Biochar from biomass residue with porous structure is an important derivative due to the high SSA and abundant oxygen-containing functional groups render excellent adsorbing ability [23, 26]. Pyrolytic carbonization is a possible thermochemical treatment to convert the biomass to biochar which shows better adsorbing ability than the biomass to POPs or metal ions in water for the advanced treatment [27, 28]. The carbonization temperature condition and the raw materials will affect the properties of the biochar, i.e., pore distribution, functional group distribution, and yield. Since the high temperature and protective atmosphere will cause a high SSA, aromaticity, and carbonization [29, 30], most of the previous reports focused on the high-temperature treatment of biomass with a protective atmosphere and showed highly absorbing ability to metal ions or organic pollutants. For example, the phosphorus from the solution could be removed by melamine-modified sugarcane bagasse bifunctional biochar material at 800 °C [31]. Potassium hydroxide-modified bagasse biochar prepared at 600 °C had adsorption of imidacloprid [32]. Eucalyptus biochar obtained by pyrolysis annealing under 800 °C nitrogen protection could remove phenol in wastewater from petroleum refineries [33], and pinecone-derived biochar (600 °C) can be defluorinated [15]. However, the costly energy and equipment associated with the preparation of synthetic porous biochar under high-temperature protective atmospheres are not advantageous to their mass production for industrial application.

Furthermore, in order to improve the adsorption ability, alkali, such as potassium/sodium hydroxide (KOH/NaOH), was often employed as an activator for the generation of mesoporous structure and enriching surface functional groups of carbon materials due to its low cost and being more environmentally friendly [26, 34–37]. The activation process produced a large number of oxygen-containing functional groups through synergistic effects, mainly hydroxyl groups, by using carbon–oxygen bonds and alkalinity [26, 38, 39]. The produced carbon materials usually showed highly SSA and porous structure, yet a high-temperature annealing process and a protective atmosphere were necessary during the reaction process.

In the current work, the sugarcane bagasse was employed as the precursor for biochar production. The carbonization process was carried out at a mild temperature (300 and 400 °C) without using protective gas. At this temperature, the hemicellulose and cellulose, the main components of biomass, are almost pyrolyzed to completion, respectively. The activation process by NaOH at such a mild temperature was also studied. The mechanism of NaOH-biochar material formation was investigated by means of thermal analysis, SSA and porosity analysis, infrared spectroscopy, and scanning electron microscopy (SEM). The adsorption ability of the produced biochar samples was studied. Rhodamine B (RhB) and chromium (III) ions (Cr(III)) which were the typical POPs and metal ions that possibly oxide to toxic Cr(VI) were employed as the target pollutants in water [40, 41]. It was found that the NaOH activation could substantially improve the adsorption ability and the adsorption mechanism was preliminarily explored. Overall, a simple and efficient preparation approach for sugarcane bagasse–based biochar/NaOH composite materials was proposed. It not only solves the problem of excessive accumulation of agricultural waste on the land, but also provides an economically viable idea for the industrial production of biochar materials.

2 Experimental

2.1 Biochar and chemically modified biochar preparation

The biochar precursor used in this experiment was the natural sugarcane bagasse raw (SCR) obtained from the commercial market in Guangzhou. The preparation procedures are detailed as follows: (1) SCR was rinsed with deionized (DI) water to remove impurities adhering to the surface, and subsequently, dried at 60 °C in an oven. (2) Afterward, the biomass was pretreated by immersing in NaOH aqueous solution (0.1 mol/L) for 24 h. The NaOH-modified dried sugarcane precursor (ASCR) was obtained. (3) ASCR was pyrolyzed at the desired temperatures (300 and 400 °C) without protective gas for 2 h. (4) The control samples were synthesized in the same process using DI water to replace the NaOH solution. (5) All as-prepared biochars above were rinsed with DI water until the pH was stable, followed by drying at 60 °C and subsequently stored. The control samples synthesized at 300 and 400 °C were denoted as SCB300

and SCB400, while the modified samples were denoted as ASCB300 and ASCB400, respectively.

2.2 Characterization of biochar

The pyrolysis process of biomass was monitored by TGA/DSC (TGA/DSC3 + , METTLER TOLEDO, Switzerland). Elemental analysis of C, H, N, S, and O was detected by an organic element analyzer (EA3000, Euro Vector, Italy). Zeta potential was carried out using a zeta potential analyzer (Nano ZS, Malvern, USA) to identify the surface charge of biochar. The pH was acquired using a pH meter (FE28, METTLER TOLEDO, Switzerland). The crystal structure was examined with an X-ray diffractometer (D8 ADVANCE, Bruker, Germany) with Cu Kα radiation (0.1541 nm) from 5 to 90°. The Fourier transform mid-infrared spectrum was used for identifying functional groups with KBr (Nicolet IS 50, Thermo Fisher, USA). The morphology of biochar was studied by a field emission scanning electron microscope (SU8220, Hitachi, Japan). The SSA and pore size distribution (PSD) were measured by an automatic fast specific surface and porosity analyzer (ASAP 2460, Micromeritics, USA).

2.3 Liquid-phase adsorption

Batch experiments were carried out in DI water at around 23 ± 1 °C (pH is approximately 7) to investigate the adsorption ability, which was conducted by placing 5 mg of the biochar into 10-mL centrifuge tubes containing 3 mL Cr(III) or RhB of different concentrations (1–16 ppm) respectively, followed by shaking in a constant temperature oscillator (THZ-B, Blue Instrument Technology, China) at 100 rpm for 2 h. The DI water was employed as a blank solution similarly. After sampling at a specific time, the supernatant was separated through a 0.22-μm filter. The concentration of Cr(III) and RhB was measured by inductively coupled plasma mass spectrometry (ICAP RQ, Thermo Fisher, USA) and an ultraviolet–visible near-infrared spectrophotometer (UV-3600 Plus, SHIMADZU, Japan) at 556 nm, respectively. The adsorption ratio and amount of Cr(III) and RhB were calculated using Eqs. (1) and (2), separately.

$$r_{\mathrm{Cr(III)/RhB}} = \left(C_0 - C_e\right)/C_0 \times 100\% \tag{1}$$

$$Q_{\mathrm{Cr(III)/RhB}} = \left(C_0 - C_e\right) \times V/M_0 \tag{2}$$

where C_0 and C_e (mg/L) are the initial and equilibrium Cr(III) and RhB concentrations in a solution, respectively, and V(L) is the volume of Cr(III) and RhB solution; M_0 (g) is the initial dry weight of the adsorbent. All the results were expressed as the mean value of duplicate measurements.

3 Results and discussion

3.1 TG/DTG analysis of biomass and chemical-modified biomass

The carbonization process of the SCR and ASCR was monitored using thermogravimetry/difference thermogravimetry (TG/DTG) shown in Fig. 1. According to the current

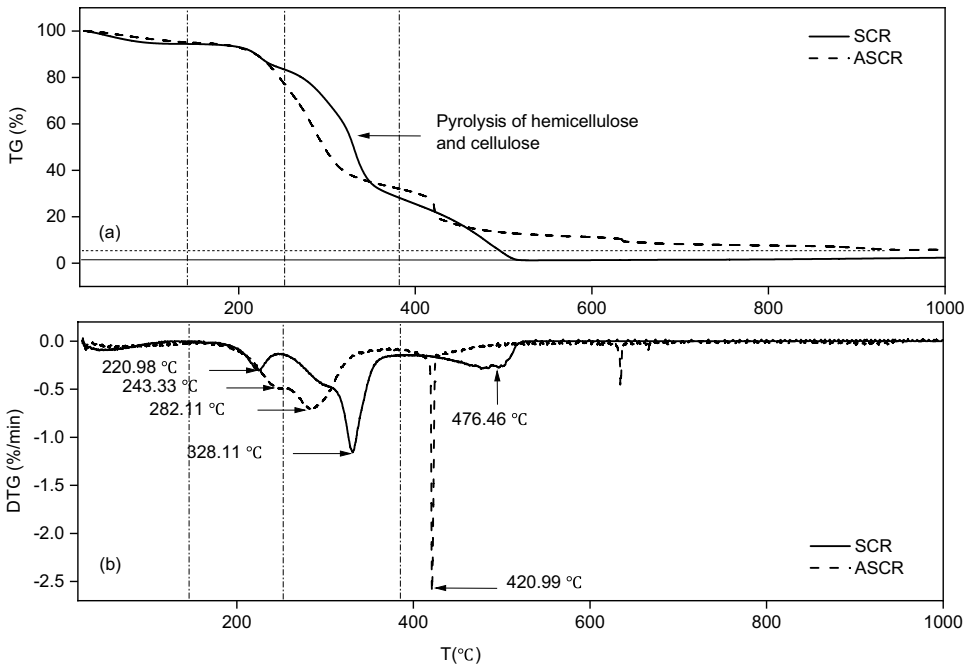

Fig. 1 **a** TG; **b** DTG thermogram of SCR (sugarcane bagasse raw) and ASCR (NaOH-modified sugarcane precursor) between 30 and 1000 °C at a heating rate of 10 °C/min without protective gas

knowledge, water evaporation, hemicellulose, cellulose, and lignin volatilization, sequentially, were observed over the entire range of biomass pyrolysis [42–44]. In the present work, hemicellulose (120–380 °C), cellulose (380–550 °C), and lignin pyrolysis occurring over the entire range were observed in SCR. Previous work showed that the main pyrolysis stage of all three components above played an important role in the initial coke formation determining the adsorption property during the mild carbonization process [45, 46]. With the progressive pyrolysis, most of the organic matter remained except hemicellulose at 300 °C, while most of the cellulose was volatile and escaped until 400 °C, remaining a backbone-like carbon structure [23]. As such, the modified sample at 400 °C could have preferable pore distribution with excellent functional groups. A smaller weight loss (> 220 °C, especially) and a slight shift to a lower temperature of DTG curves were presented in ASCR versus SCR. As can be observed in Fig. 1b, the characteristic peaks of the maximum weightless rate of hemicellulose and cellulose were displaced to lower temperatures, and Han et al. pointed out that this could be due to the metal ions with alkali modification [47]; likewise, Jais et al. proposed the NaOH impregnation contributed to the dissolution of hemicellulose and cellulose [26]. It has, also, been reported that alkali pretreatment reduced clogged pores by clearing up impurities such as tar [48]. More ash content in the residue at 300 and 400 °C of ASCR was formed as that of SCR based on previous literature, in which the metal ions and oxides contained therein may be driving factors in pollutant adsorption [37, 38]. Consequently, ASCB synthetic materials with greater porosity, and abundant inorganic and organic components can be manufactured at a lower temperature (300 and 400 °C).

3.2 Elemental distribution and zeta potential

Several properties including element compositions, zeta potential, H/C (aromaticity and carbonization), O/C (hydrophilic), and (O + N)/C (polarity) of biochars are presented in Table 1. The zeta potential (pH = 8.34–9.85) of SCB and ASCB indicated that the surface of biochars had a negative charge attributing to the surface basic functional groups of biochars and probably conducive to the adsorption of cationic pollutants [49]. The negatively charged surface groups attracted the cations in the environment so that high cation exchange capacity was expressed in biochar [23, 50]. Xiao et al. reported that along with the increase in carbonization temperature, the carbon element was enriched with enhanced aromaticity, while the hydrophilicity (< 350 °C) and polarity were weakened in the biochar [51], which was due to the aliphatic carbon and aromatic carbon with low aromaticity in biomass. As the pyrolysis reaction proceeded, oxygen and hydrogen were dissociated, and new aromatic carbon was formed, which improved with temperature increasing, forming regular aromatic carbon fragments [48, 52]. The aromatic carbon structure of biochar provided a possibility to bind to the organic compounds with aromatic structures in the environment through the π-π electron donor–acceptor action [50]. During pyrolysis, meanwhile, a large number of groups are volatilized and left from the surface of the aromatic carbon while non-polar and hydrophobic groups remained on the biochar surface leading to increased polarity. Both SCB and ASCB were enriched in carbon (58.97 to 62.31%, 57.93 to 63.35%, respectively, in this work) with the pyrolysis temperature rising (300–400 °C) representing that the carbonization degree of biochar was enhanced that was consistent with what the carbonization process described in the TG. Complementary to the increase in carbon content was the decrease in atomic ratios of H/C, O/C, and (O + N)/C in biochar drawn from several research [51, 53–55]. Consistent with this, the H/C ratio of SCB and ASCB was decreased from 0.06 to 0.05 and 0.08 to 0.05, respectively, which implied higher aromatic biochar production with temperature increasing; meanwhile, the ratios of O/C and (O + N)/C of SCB and ASCB were decreased, indicating that the hydrophilicity of the surface reduced due to the disappearance of hydrophilic functional groups and the decreased polarity of SCB and ASCB. Upon NaOH activation to generate ASCB (300 and 400 °C), the polarity and hydrophilicity were weakened, yet aromaticity seemed to be no different.

Table 1 pH, zeta potential, organic element distribution, specific surface area, total pore volume, micropore volume, and average pore size of SCB (sugarcane biochar) and ASCB (NaOH-modified sugarcane biochar).

Biochar	pH	Zeta potential	C (%)	H (%)	N (%)	O (%)	H/C	O/C	(O + N)/C	S_{BET}*	V_t**	V_{micro}***	D_p****
SCB300	9.85	− 19.10	58.97	3.39	1.06	22.02	0.06	0.37	0.39	0.35	8.80e − 004	1.15e − 004	10.41
SCB400	9.02	− 21.10	62.31	2.92	1.22	19.96	0.05	0.32	0.34	0.86	1.39e − 003	3.48e − 004	6.68
ASCB300	8.82	− 10.60	57.93	4.63	0.51	18.44	0.08	0.32	0.33	0.52	1.88e − 003	7.30e − 005	14.68
ASCB400	8.34	− 41.00	63.35	3.35	0.44	15.94	0.05	0.25	0.26	8.59	2.71e − 002	2.12e − 003	4.94

S_{BET}*, m^2/g, the specific surface area; V_t**, m^3/g, the total pore volume; V_{micro}***, m^3/g, the micropore volume; D_p****, nm, average pore size.

3.3 XRD, FTIR analysis

Two wide peaks at around 22 and 41° were observed with XRD shown in Fig. 2a, corresponding to the (002) and (101) crystal plane diffraction of carbon. Due to the ordered graphite structure which could facilitate the formation of π-π bond [34], the adsorption of pollutants containing a conjugated structure could be encouraged in the adsorption. The increment of pyrolysis temperature or the NaOH treatment seemed not to affect the carbon backbone structure. The peaks of inorganic salts in ash such as $CaCO_3$, SiO_2, and KCl can also be observed, similar to the previous study [14], which might play a driving role in the removal of metal ions [37]. Abundant characteristic peaks were observed in both SCB and ASCB in FTIR analysis shown in Fig. 2b, which could provide active sites so as to enhance the adsorption performance [35]. The peaks corresponding to the -CH_n vibrations (2933 cm^{-1}, 2860 cm^{-1}, 1373 cm^{-1}) and C = O (1713 cm^{-1}) were gradually weakened; meanwhile, C–O–C (1171 cm^{-1}) of pyranose ring skeletal bonding ketone and carbonyl C = O (1512 cm^{-1}) vibration peak of cellulose disappeared, from contrast with SCB300 and SCB400, while C = C (1608 cm^{-1}) increased. This phenomenon was supposed to be the pyrolysis volatilization of cellulose and hemicellulose from 300 up to 400 °C [44], which was consistent with the pyrolysis process of the TG-DTG curve. Correspondingly, the polarity of biochar was gradually weakened during the pyrolysis process, and the degree of aromatization was gradually increased, resulting in the adsorption capacity increasing accordingly [52, 56]. -OH (3408 cm^{-1}) and C–OH (1031 cm^{-1}) were slightly increased after NaOH activation, representing that the oxygen functional group of biochar was enhanced; this was similar to the results of reported research [26]. Similarly, the displacement of C = O (1713 to 1698 cm^{-1}) could be caused by the activation process. The increase in pyrolysis temperature reduced the polarity and enhanced aromatization, and the alkali pretreatment increased the oxygen-containing functional groups on the surface of biochar (mainly -OH), contributing to the enhanced adsorption capacity [26, 42].

3.4 Surface analysis and pore distribution

According to the previous literature [34, 38], the alkali modification, i.e., NaOH, could optimize some blocking pores to open holes and increase the porosity of the material. As mentioned in the Jais et al. study, during NaOH activation, the main reaction that occurs refer to Eqs. (3)–(5):

$$6NaOH + 2C \rightarrow 2Na + 2Na_2CO_3 + 3H_2 \quad (3)$$

$$Na_2CO_3 \rightarrow Na_2O + CO_2 \quad (4)$$

$$2Na + CO_2 \rightarrow Na_2O + CO \quad (5)$$

In the process of pyrolysis, the reaction between NaOH and carbon could promote the reduction of sodium ions to metal sodium and the formation of sodium carbonate (Na_2CO_3), while the hydroxyl anion will become hydrogen (H_2), and then, the decomposition of sodium carbonate (Na_2CO_3), and the embedding of metal sodium (Na) in the carbon backbone can produce carbon dioxide (CO_2) and carbon monoxide (CO) to generate smaller mesopores and micropores [26], resulting in the increased SSA and the enriched functional group species as well as the adsorption capacity [37, 57]. Accordingly, the higher ash content of ASCB might be due to the produced sodium oxide (Na_2O) and carbonates during the alkali modification [36].

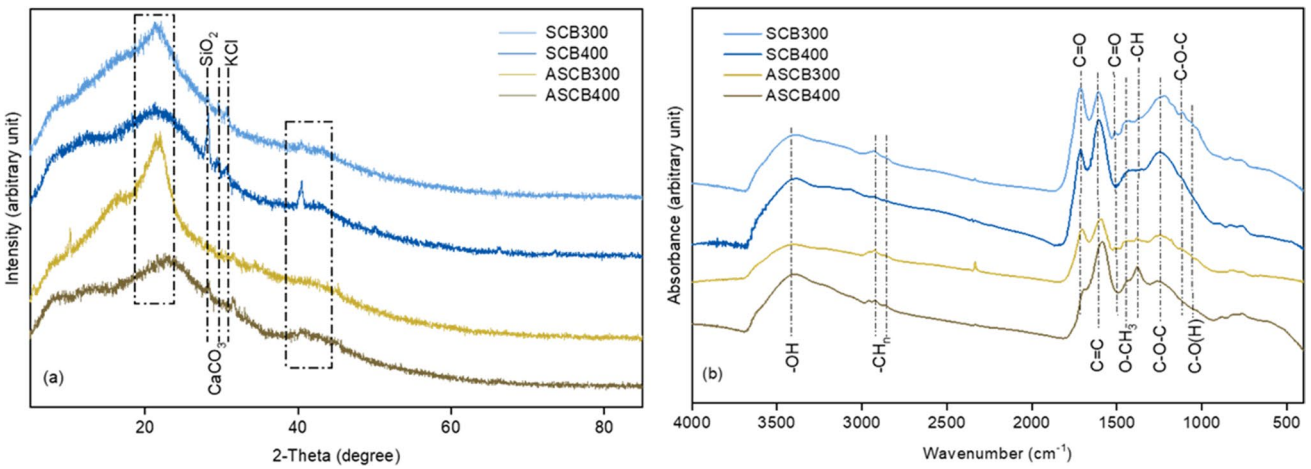

Fig. 2 **a** XRD; **b** FTIR spectral analysis for the SCB (sugarcane biochar) and ASCB (NaOH-modified sugarcane biochar) before adsorption. The numbers after "SCB" and "ASCB" represent the pyrolysis temperatures

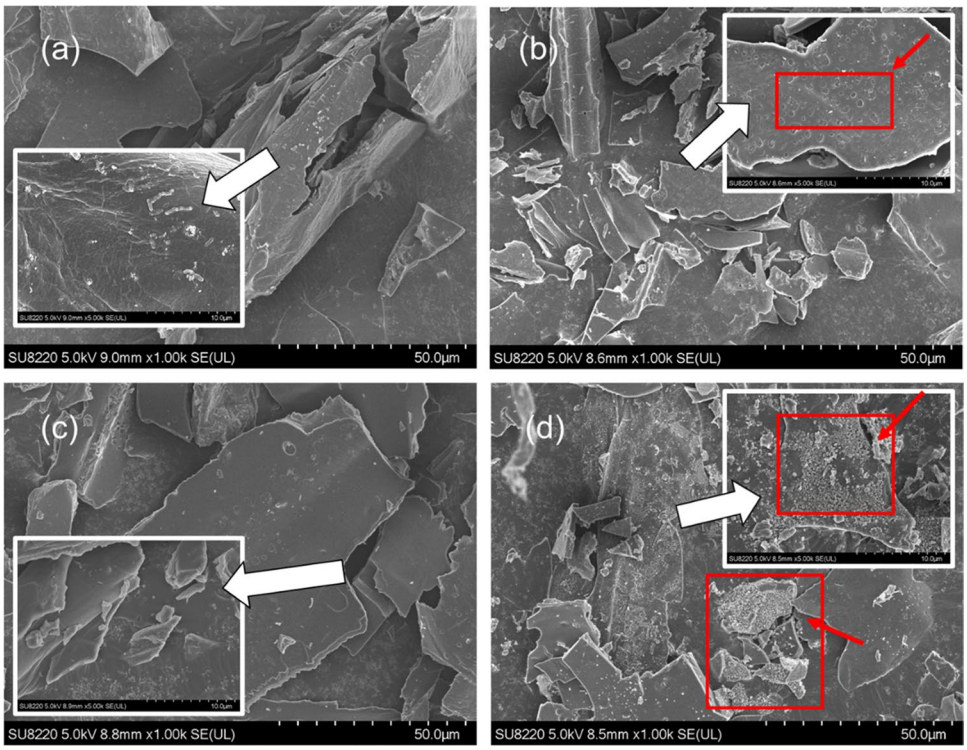

Fig. 3 SEM images of sugarcane biochar (**a** SCB300; **b** SCB400), and NaOH-modified sugarcane biochar (**c** ASCB300 and **d** ASCB400) before adsorption. The image indicated by the white arrow is a 5.00 K × magnification. The bold red arrow points to a typical pore morphology distribution

The morphology of biochar is shown in Fig. 3. The smooth surface of SCB300 and fragmentation distribution of SCB400 indicated that fiber chain structures, as well as the collapse of the carbon network, were destroyed with the increment of pyrolysis temperature, and accordingly, quantities of pore structure and inner pore appeared on the surface. Meanwhile, uneven open pores were observed on the surface of ASCB300, and by the increment of pyrolysis temperature, a considerable number of non-uniform arranged pore structures and cracks appeared on the surface of ASCB400 obviously, which was consistent with the relatively high SSA and wide pore structure distribution after activation (Fig. 4). As exhibited in Fig. 3 and Table 1, from the nitrogen adsorption–desorption isotherms, type II adsorption isotherm, and

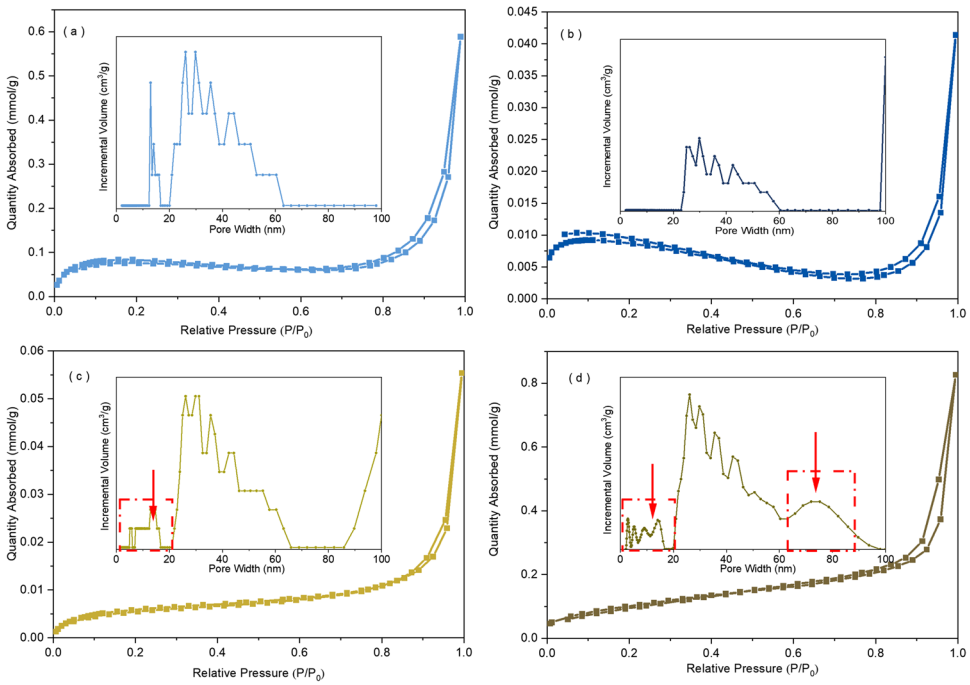

Fig. 4 Nitrogen adsorption–desorption isotherms and pore diameter distribution of sugarcane biochar (**a** SCB300; **b** SCB400), and NaOH-modified sugarcane biochar (**c** ASCB300 and **d** ASCB400). The red arrows show the more pronounced change in the pore size distribution of ASCB compared to SCB

H2(a) type hysteresis loop indicated that the material had a mesoporous structure consisting with SEM results. Distinctly, as the temperature rises, SCB400 had less mesopore distribution (2–20 nm) versus SCB300, and the 20–60-nm meso-macropore distribution was, also, reduced, probably due to the collapse of the carbon structure resulting in clogging of partial pores; meanwhile, the increase in the total volume of micropores exhibited the amount of new micropores generated (Table 1).

With the increase of pyrolysis temperature, the SSA of biochar was increased and further increased with NaOH modification; especially the SSA of ASCB400 (8.59 m^2/g) was 10 to 24 times higher than that of other biochars which was similar to the results of previous reports [35, 38]. Furthermore, all samples after alkalinization (ASCB300, ASCB400) were observed, not only to maintain and motivate the original meso-macropore distribution (20–100 nm), but also to generate numerous mesopore distribution (2–20 nm) due to the gas species in Eqs. (3)–(5) produced. The average pore diameter of ASCB400 was 4.94 nm, which was smaller than that of ASCB300 (14.68 nm), SCB300 (10.41 nm), and SCB400 (6.68 nm). NaOH activation chemically etched the dense carbon network, and a large number of 2–20-nm mesopores appeared inside the biochar; thus, the mass transfer and more adsorption and filling sites were promoted, which was conducive to the removal of pollutants [34, 35, 37]. Likewise, Wei-Cong Qian et al. synthesized bamboo-biochar material with NaOH modification determined to have an SSA of 1.40 m^2/g [58]. As can be observed at low temperature (< 400 °C), the biochar after NaOH treatment in this study, with a slight advantage of SSA than partially previous literature reported, might present superior adsorption capacity.

The XPS of SCB300 and SCB400 are shown in Figs. S3 and S4. Deconvolution of the data indicated three possible energy of the carbon bonds, including the sp^2 and sp^3 C–C, C-O, and C = O bonds, responsible for the 284.6, 286.2, and 288.7 eV [37, 42]. The binding of N at 399.6 eV indicated the appearance of C-N–H bonds of the biochars. The detectable 1 s of Na at 1071.1 eV implied its stabilization during the alkali pretreatment. This stabilization was achieved around the polar functional groups, such as the -OH. A small peak at 536.7 eV was observed in ASCB400, instead of ASCB300. Based on the NIST Spectral Library, this peak came from the Auger energy of O that could be considered more stabilized of Na on the biochar.

3.5 Analysis of adsorption property and possible mechanism

The increased SSA attributed to the alkali treatment resulted in more adsorption sites, so it could improve the adsorption capacity of the biochar possibly. The adsorption ability was estimated toward RhB and Cr(III), which were the representative organic and metal pollutants. As exhibited in Fig. 5, the liquid adsorption isotherm and the removal of RhB and Cr (III) demonstrated that the samples exhibited a convex curvature, indicating a type I (according to the IUPAC standard) isotherm to RhB. It demonstrated that the adsorption approached a maximum adsorbed concentration, the saturation capacity because the higher concentration of RhB caused the smaller degree of adsorption. Meanwhile, for Cr(III), the samples exhibited a concave curvature, representing the type III isotherms, from which a high concentration of Cr(III) was advantageous to the larger degree of adsorption. As shown in Fig. 5c and d, both r_{RhB} and $r_{Cr(III)}$ of the ASCB samples were higher than those of SCB in various pollutant concentrations, indicating the ASCB had stronger adsorption ability than the SCB, and demonstrating that alkali pretreatment had improved the adsorption ability of biochar.

Previous research has established that a variety of mechanisms including physical adsorption, complexation, ion exchange, and precipitation combine to influence the adsorption behavior of biochar on heavy metal ions [25, 42, 59]. Based on the above discussion, a high SSA and optimization of pore distribution attributed to chemically regulated biochar of NaOH provided more physical adsorption sites for the adsorption of Cr (III); moreover, negative charge distribution on the surface could motivate the electrostatic attraction, especially for ASCB, with more negative surface potential, preferred adsorption of cations [38]. As indicated in Fig. S1, the complexes of Cr(III) were formed on the surface of biochar. The vibration of -OH was weakened and shifted toward the high wavenumber with a step of 13–29 cm^{-1}. In addition, the peaks responsible for the Cr_2O_3 (1384 and 616 cm^{-1}) and Cr $(OH)_3$ (1464, 1378, and 722 cm^{-1}) were observed, indicating the stabilization of adsorbed Cr(III) [25, 42, 60]. This view is supported by Batool et al. who claimed that Cr(III) and -OH formed stable complexes of Cr $(OH)_3$ and Cr_2O_3 on biochar [59, 61]. Moreover, the 3p binding energy of Cr(III) could be observed at 577.5 and 587.1 eV in XPS (Fig. S5, S6), confirming the appearance of Cr_2O_3 and Cr $(OH)_3$ equally [38]. Thus, Cr(III) in an aqueous solution was successfully adsorbed on the biochar. The various inorganic components of the aforementioned alkali-regulated biochar, such as KCl, $CaCO_3$, and Na_2O, possessed the potential to exchange ions with Cr(III) in the aqueous phase (Figs. 1 and 2). Interestingly, superior micro-mesoporous distribution and larger SSA were presented on ASCB400 than on ASCB300, while the adsorption amount of Cr(III) was comparable in this work inferring that SSA and other factors such as functional group distribution and charge distribution compound affected the adsorption of Cr(III) on NaOH-activated biochar cooperatively. As a possible interpretation, the appearance of Na in the biochar

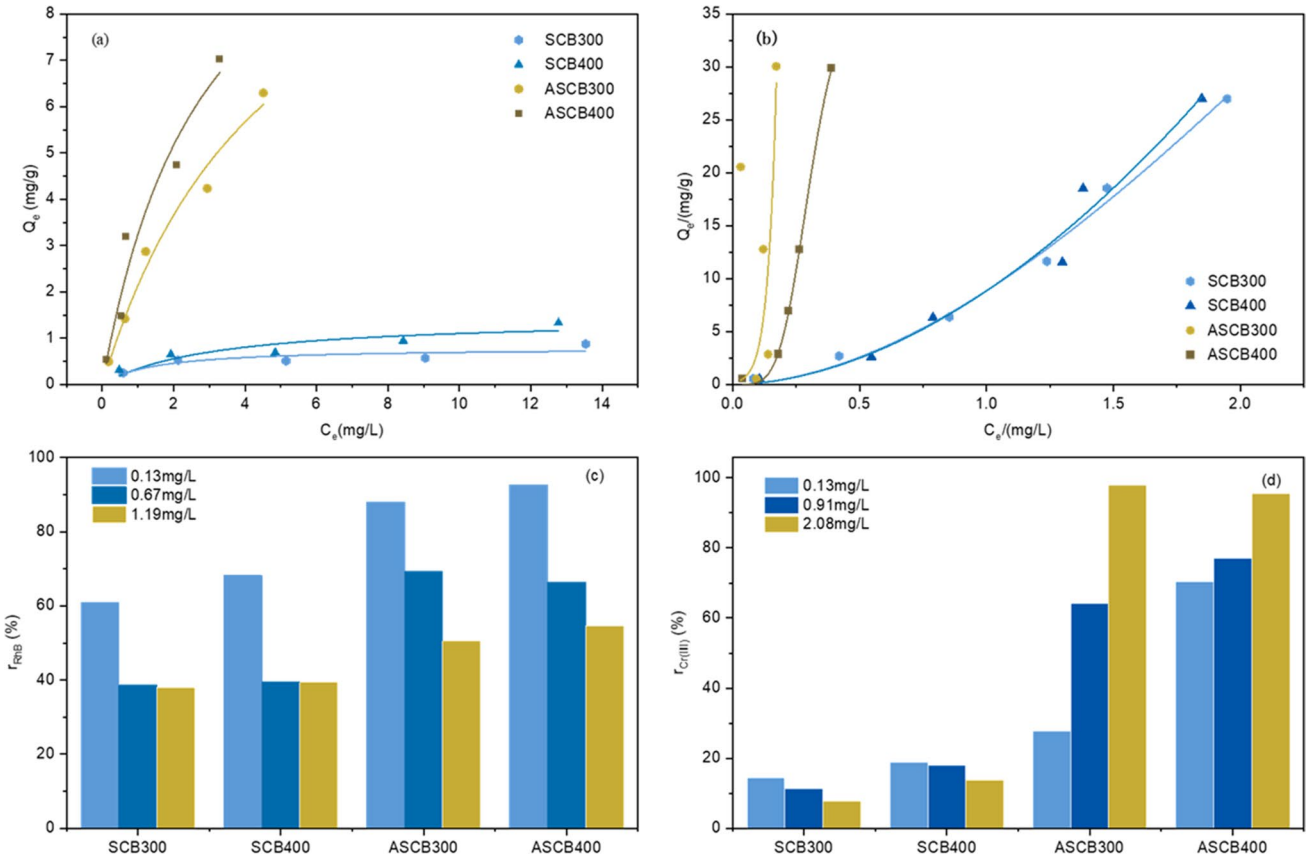

Fig. 5 Sorption isotherm and removal ratio of RhB (**a**, **c**); Cr (III) (**b**, **d**) from 0.09 to 2.08 mg/L solutions by 5 mg SCB (sugarcane biochar) and ASCB (NaOH-modified sugarcane biochar) at 25 °C and pH of 6.98

resulted in the competitive adsorption to Cr(III); thus, the ASCB400 with more Na ions showed smaller adsorbed amount to Cr(III) as compared to the ASCB300 (Fig. 5). Differently, the adsorption mechanism of RhB was mainly controlled by pore filling, π-π interaction, H bond, and electrostatic attraction [34, 35]. The SSA of ASCB300 and ASCB400 were 0.52 and 8.59 m^2/g, respectively, which were 1.5 times and 10 times higher than the original ones, and the TPV was increased by 19 times and 2 times, respectively. Moreover, the pore distribution was optimized; more micropores and narrow mesopores were raised in ASCB, providing pore-filling adsorption sites for the adsorption of pollutants. Furthermore, the ordered graphitized structure shown in micropore generating XRD contributed to the formation of π-π bonds [34]; the enhanced aromatization derived from FTIR and elemental analysis was also favorable to the formation of π-π bonds with aromatic structured organics [35], as well as the distribution of negative surface charge for the electrostatic attraction of RhB [34]. The vibration of -OH shifted toward a high wavenumber direction with a step of 11–14 cm^{-1} of before and after RhB adsorption from Fig. S2, probably due to the attachment of RhB molecules to hydrogen bonds with -OH [35]. In addition, the vibration from -CH_n (2840–2920 cm^{-1}) was increased, confirming its adsorption on biochars. Chen et al. proposed that the high SSA and pore size distribution provided further pore filling points, and functional groups offering H-bond between biochar and RhB, and the imine nitrogen of RhB maintained a positive charge through electrostatic interaction to improve its adsorption on the biochar surface [35]. Referring to Figs. S7 and S8, the increment of 1 s peak of N also confirmed the RhB adsorption. Under the experimental conditions specified in this study, the optimum adsorption capacities of alkali-treated modified biochars (ASCB300 and ASCB400) for Cr (III) were 30.06 mg/g and 29.90 mg/g, respectively; the optimum adsorption capacities for RhB were 6.29 mg/g and 7.03 mg/g, which was superior over the unmodified biochar adsorption capacity (RhB: 6–7 times; Cr (III): 1–2 times). Therefore, under the combined effect of the above factors, the biochar with alkalinization rendered preferable adsorption capacity of Cr(III) and RhB. A monolayer coverage adsorption per unit specific surface area (Q_m/S_{BET}) was calculated; also, a comparison with previous studies is shown in Table 2. As seen from the removal rate (Fig. 5c, d), while RhB uptake approached the saturation capacity and a high concentration of RhB reduced the degree of adsorption,

Table 2 Data of Q_m (maximum adsorption capacity)/S_{BET} (specific surface area) of modified biochar for different adsorbates

Adsorbent	Adsorbate	pH	Temp.(°C)	S_{BET} (m^2/g)	$Q_{max}{}^*/S_{BET}$ (mg/m^2)	Reference
NaOH-sugarcane BC-300 °C	RhB	Without adjustment	25	0.52	12.10	Present work
	Cr (III)		25		57.79	
NaOH-sugarcane BC-400 °C	RhB		25	8.59	0.82	
	Cr (III)		25		3.48	
HCl- bamboo hydrochar-200 °C	Methylene blue	-**	30	31.60	8.04	[58]
NaOH-bamboo BC-200 °C				1.40	191.70	
Acid/alkali-bamboo BC-200 °C				26.25	24.95	
KOH- corn cobs hydrochar-230 °C	Ammonium nitrogen	-	25	3.18	2.16	[59]
KOH- corn cobs hydrochar-260 °C				5.26	1.70	
KOH- douglas fir BC 900–1000 °C	Cr (VI)	-	25	1049.00	0.08	[37]
NaOH-fir wood BC-450 °C	Methylene blue	Without adjustment	25	2406.00	0.28	[49]
NaOH-fir wood BC 450 °C -2				1672.00	0.44	
Sugarcane biochar/ iron oxide composite 110 °C	Cr (VI)	Without adjustment	25	342.36	3.31	[42]
Sodium alginate/NaOH sugarcane BC-80 °C	Malachite green	-	-	82.23	0.70	[43]
NaOH-tea BC-700 °C	Methylene Blue	10	25	178.00	0.59	[34]
	Orange II	2			0.54	
KOH- corn straw BC-500 °C	Cr (VI)	-	30	2183.80	0.05	[60]
Edible fungus-NaOH BC-600 °C	RhB	-	25	1598.90	0.57	[35]
NaOH-citrus peel BC-500 °C	Cd (II)	-	25	148.41	1.24	[38]

*Q*max*, maximum adsorption capacity; -**, not mentioned

the high concentration of Cr (III) was advantageous to the larger degree of adsorption until constant, which was due to the different adsorption mechanisms of RhB and Cr (III) on the biochar. It might be suggested that the removal of RhB was mainly controlled by physical adsorption: due to the limited number of active adsorption sites in the adsorbent, the excessive solute density of RhB resulted in its complete consumption until the dynamic saturation adsorption; thus, the removal rate of RhB decreases when the initial concentration of RhB increases. Differentially, the adsorption of Cr (III) on alkali-modified biochar might be based on chemisorption, showing a gradual increase with the initial concentration as well as continuous precipitation producing until a constant state [38]. The schematic of possible adsorption mechanism of modified biochar for Cr (III) and RhB is shown in Fig. 6.

4 Conclusions

In this work, NaOH was used as an activator to modify sugarcane bagasse biochar. The SSA and TPV of the modified ASCB were significantly optimized (10, 1.5 times; 19, 2 times, respectively), which proved the pore-forming effect

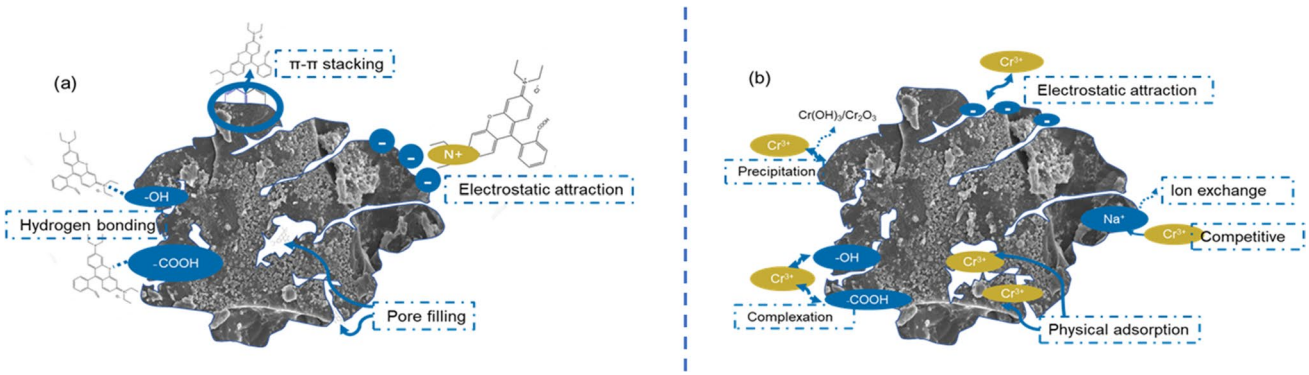

Fig. 6 Schematic of possible adsorption mechanism of **a** RhB and **b** Cr(III) by NaOH-modified sugarcane biochar

of NaOH in the activation process (both mesopore and micropore). Oxygen-containing functional groups (mainly C–OH) were expanded, especially on the activated one at 400 °C which showed an optimized pore structure with uneven distribution. In addition, the adsorption performance of each biochar for RhB and Cr(III) was investigated. The maximum adsorption amounts of ASCB300 and ASCB400 for RhB and Cr(III) were 6.29, 7.02 mg/g; and 30.06, 29.90 mg/g, respectively (6–7 times for RhB before modification and 1–2 times for Cr(III) before activation), which was higher than that before modification. Moreover, a larger adsorption capacity per unit specific surface area of monolayer coverage was observed on alkalinized biochar than in other literature. Finally, the possible adsorption mechanisms were initially explored; pore filling, π-π interaction, and electrostatic attraction were the main mechanisms of the RhB adsorption process, while pore filling might be the dominant physical adsorption. The adsorption mechanisms of Cr(III) were mainly physical adsorption, complexation, precipitation, and cation exchange, while chemisorption should be the dominant one.

Supplementary Information The online version contains supplementary material available at https://doi.org/10.1007/s13399-022-03009-8.

Author contribution Chunxiao Yang and Haoyi Wu: conceptualization, methodology, data curation, writing — original draft, investigation, project administration, funding acquisition, writing — review and editing. Xianzhi Zeng, Zhongshuo Pan, Huidan Tan, and Shan Chen: investigation, validation, formal analysis, visualization. All the authors approved the submission.

Funding This work was supported by the financial support from Guangdong Natural Science Foundation (No. 2021A1515010179).

Data availability The data used to support the findings of this study are included within the article.

Declarations

Conflict of interest The authors declare no competing interests.

References

1. Tee GT, Gok XY, Yong WF (2022) Adsorption of pollutants in wastewater via biosorbents, nanoparticles and magnetic biosorbents: a review. Environ Res 212(Pt B):113248
2. Arefi-Oskoui S, Khataee A, Jabbarvand Behrouz S, Vatanpour V, Haddadi Gharamaleki S, Orooji Y, Safarpour M (2022) Development of MoS2/O-MWCNTs/PES blended membrane for efficient removal of dyes, antibiotic, and protein, Separation and Purification Technology 280
3. Shakya A, Agarwal T (2019) Removal of Cr (VI) from water using pineapple peel derived biochars: adsorption potential and re-usability assessment, Journal of Molecular Liquids 293
4. Orooji Y, Nezafat Z, Nasrollahzadeh M, Kamali TA (2021) Polysaccharide-based (nano)materials for Cr (VI) removal. Int J Biol Macromol 188:950–973
5. Sharma S, Mittal A, Chauhan NS, Saini S, Yadav J, Kushwaha M, Chakraborty R, Sengupta S, Kumari K, Kumar N (2022) Mechanistic investigation of RhB photodegradation under low power visible LEDs using a Pd-modified TiO_2/Bi_2O_3 photocatalyst: experimental and DFT studies, Journal of Physics and Chemistry of Solids 162
6. Chen C, Liu P, Li Y, Tian H, Zhang Y, Zheng X, Liu R, Zhao M, Huang X (2022) Electro-peroxone enables efficient Cr removal and recovery from Cr (III) complexes and inhibits intermediate Cr (VI) generation in wastewater: performance and mechanism. Water Res 218:118502
7. Karimi-Maleh H, Ranjbari S, Tanhaei B, Ayati A, Orooji Y, Alizadeh M, Karimi F, Salmanpour S, Rouhi J, Sillanpaa M, Sen F (2021) Novel 1-butyl-3-methylimidazolium bromide impregnated chitosan hydrogel beads nanostructure as an efficient nanobio-adsorbent for cationic dye removal: kinetic study. Environ Res 195:110809
8. Orooji Y, Mohassel R, Amiri O, Sobhani A, Salavati-Niasari M (2020) Gd2ZnMnO6/ZnO nanocomposites: green sol-gel autocombustion synthesis, characterization and photocatalytic degradation of different dye pollutants in water, Journal of Alloys and Compounds 835
9. Gholami P, Dinpazhoh L, Khataee A, Orooji Y (2019) Sonocatalytic activity of biochar-supported ZnO nanorods in degradation of gemifloxacin: synergy study, effect of parameters and phytotoxicity evaluation. Ultrason Sonochem 55:44–56
10. Keyikoglu R, Khataee A, Lin H, Orooji Y (2022) Vanadium (V)-doped ZnFe layered double hydroxide for enhanced sonocatalytic degradation of pymetrozine, Chemical Engineering Journal 434
11. Li Y, Zhou Y, Wang R, Chen Z, Luo X, Wang L, Zhao X, Zhang C, Yu P (2022) Removal of aflatoxin B1 from aqueous solution using amino-grafted magnetic mesoporous silica prepared from rice husk. Food Chem 389:132987
12. Mancinelli M, Stevanin C, Ardit M, Chenet T, Pasti L, Martucci S (2022) PFAS as emerging pollutants in the environment: a challenge with FAU type and silver-FAU exchanged zeolites for their removal from water, Journal of Environmental Chemical Engineering
13. Li Y, Wang X, Duan Z, Yu D, Wang Q, Ji D, Liu W (2022) Zn/Co-ZIFs@MIL-101(Fe) metal–organic frameworks are effective photo-Fenton catalysts for RhB removal, Separation and Purification Technology 293
14. Bai X, Zhang M, Niu B, Zhang W, Wang X, Wang J, Wu D, Wang L, Jiang K (2022) Rotten sugarcane bagasse derived biochars with rich mineral residues for effective Pb (II) removal in wastewater and the tech-economic analysis, Journal of the Taiwan Institute of Chemical Engineers 132
15. Khan BA, Ahmad M, Iqbal S, Bolan N, Zubair S, Shafique MA, Shah A (2022) Effectiveness of the engineered pinecone-derived biochar for the removal of fluoride from water. Environ Res 212(Pt D):113540
16. Jeong CY, Dodla SK, Wang JJ (2016) Fundamental and molecular composition characteristics of biochars produced from sugarcane and rice crop residues and by-products. Chemosphere 142:4–13
17. Guga S, Xu J, Riao D, Li K, Han A, Zhang J (2021) Combining MaxEnt model and landscape pattern theory for analyzing interdecadal variation of sugarcane climate suitability in Guangxi, China, Ecological Indicators 131
18. Guo H, Huang Z, Tan M, Ruan H, Awe GO, Are KS, Abegunrin TP, Hussain Z, Kuang Z, Liu D (2021) Crop resilience to climate change: a study of spatio-temporal variability of sugarcane yield in a subtropical region, China, Smart Agricultural Technology 1

19. Montero JIZ, Monteiro ASC, Gontijo ESJ, Bueno CC, de Moraes MA, Rosa AH (2018) High efficiency removal of As (III) from waters using a new and friendly adsorbent based on sugarcane bagasse and corncob husk Fe-coated biochars. Ecotoxicol Environ Saf 162:616–624
20. Khaire KC, Moholkar VS, Goyal A (2021) Bioconversion of sugarcane tops to bioethanol and other value added products: an overview. Mater Sci Energy Technol 4:54–68
21. Valente F, Laurini M (2021) Pre-harvest sugarcane burning: a statistical analysis of the environmental impacts of a regulatory change in the energy sector, Cleaner Engineering and Technology 4
22. Mubarik S, Saeed A, Athar MM, Iqbal M (2016) Characterization and mechanism of the adsorptive removal of 2,4,6-trichlorophenol by biochar prepared from sugarcane baggase. J Ind Eng Chem 33:115–121
23. Yahya MA, Al-Qodah Z, Ngah CWZ (2015) Agricultural bio-waste materials as potential sustainable precursors used for activated carbon production: a review. Renew Sustain Energy Rev 46:218–235
24. He L, Liu Z, Hu J, Qin C, Yao L, Zhang Y, Piao Y (2021) Sugarcane biochar as novel catalyst for highly efficient oxidative removal of organic compounds in water. Chem Eng J 405
25. Qiu Y, Zhang Q, Gao B, Li M, Fan Z, Sang W, Hao H, Wei X (2020) Removal mechanisms of Cr (VI) and Cr (III) by biochar supported nanosized zero-valent iron: synergy of adsorption, reduction and transformation. Environ Pollut 265(Pt B):115018
26. Jais FM, Chee CY, Ismail Z, Ibrahim S (2021) Experimental design via NaOH activation process and statistical analysis for activated sugarcane bagasse hydrochar for removal of dye and antibiotic. J Environ Chem Eng 9(1)
27. Liu J, Yang X, Liu H, Cheng W, Bao Y (2020) Modification of calcium-rich biochar by loading Si/Mn binary oxide after NaOH activation and its adsorption mechanisms for removal of Cu (II) from aqueous solution, Colloids and Surfaces A: Physicochem Eng Aspects 601
28. Zhao J, Shen XJ, Domene X, Alcañiz JM, Liao X, Palet C (2019) Comparison of biochars derived from different types of feedstock and their potential for heavy metal removal in multiple-metal solutions. Sci Rep 9(1)
29. Almutairi AA, Ahmad M, Rafique MI, Al-Wabel MI (2022) Variations in composition and stability of biochars derived from different feedstock types at varying pyrolysis temperature, Journal of the Saudi Society of Agricultural Sciences
30. Inkoua S, Li C, Fan H, BkangmoKontchouo FM, Sun Y, Zhang S, Hu X (2022) Pyrolysis of furfural residues: property and applications of the biochar. J Environ Manage 316:115324
31. Liao Y, Chen S, Zheng Q, Huang B, Zhang J, Fu H, Gao H (2022) Removal and recovery of phosphorus from solution by bifunctional biochar, Inorganic Chemistry Communications 139
32. Ma Y, Qi Y, Yang L, Wu L, Li P, Gao F, Qi X, Zhang Z (2021) Adsorptive removal of imidacloprid by potassium hydroxide activated magnetic sugarcane bagasse biochar: adsorption efficiency, mechanism and regeneration, Journal of Cleaner Production 292
33. Singh R, Dutta RK, Naik DV, Ray A, Kanaujia PK (2021) High surface area Eucalyptus wood biochar for the removal of phenol from petroleum refinery wastewater, Environmental Challenges 5
34. Mu Y, Ma H (2021) NaOH-modified mesoporous biochar derived from tea residue for methylene Blue and Orange II removal. Chem Eng Res Des 167:129–140
35. Chen S, Zhang B, Xia Y, Chen H, Chen G, Tang S (2021) Influence of mixed alkali on the preparation of edible fungus substrate porous carbon material and its application for the removal of dye, Colloids and Surfaces A: Physicochemical and Engineering Aspects 609
36. Yu X, Liu S, Lin G, Yang Y, Zhang S, Zhao H, Zheng C, Gao X (2020) KOH-activated hydrochar with engineered porosity as sustainable adsorbent for volatile organic compounds, Colloids and Surfaces A: Physicochemical and Engineering Aspects 588
37. Herath A, Layne CA, Perez F, Hassan EB, Pittman CU Jr, Mlsna TE (2021) KOH-activated high surface area Douglas fir biochar for adsorbing aqueous Cr (VI), Pb(II) and Cd(II). Chemosphere 269:128409
38. Du H, Xi C, Tang B, Chen W, Deng W, Cao S, Jiang G (2022) Performance and mechanisms of NaOH and ball-milling co-modified biochar for enhanced the removal of Cd2+ in synthetic water: a combined experimental and DFT study, Arabian Journal of Chemistry 15(6)
39. Shin J, Kwak J, Lee YG, Kim S, Choi M, Bae S, Lee SH, Park Y, Chon K (2021) Competitive adsorption of pharmaceuticals in lake water and wastewater effluent by pristine and NaOH-activated biochars from spent coffee wastes: contribution of hydrophobic and pi-pi interactions. Environ Pollut 270:116244
40. Ye H, Zhang Y, Wei L, Feng H, Fu Q, Guo Z (2022) Waterborne Cr (3+) and Cr (6+) exposure disturbed the intestinal microbiota homeostasis in juvenile leopard coral grouper Plectropomus leopardus. Ecotoxicological and Environmental Safety 239:113653
41. Dash B, Jena SK, Rath SS (2022) Adsorption of Cr (III) and Cr (VI) ions on muscovite mica: experimental and molecular modeling studies, Journal of Molecular Liquids 357
42. Bai L, Su X, Feng J, Ma S (2021) Preparation of sugarcane bagasse biochar/nano-iron oxide composite and mechanism of its Cr (VI) adsorption in water, Journal of Cleaner Production 320
43. Das L, Das P, Bhowal A, Bhattachariee C (2020) Treatment of malachite green dye containing solution using bio-degradable sodium alginate/NaOH treated activated sugarcane bagasse charcoal beads: batch, optimization using response surface methodology and continuous fixed bed column study. J Environ Manage 276:111272
44. Yang H, Yan R, Chen H, Lee DH, Zheng C (2007) Characteristics of hemicellulose, cellulose and lignin pyrolysis. Fuel 86(12–13):1781–1788
45. Song F, Wang X, Li T, Zhang J, Bai Y, Xing B, Giesy JP, Wu F (2019) Spectroscopic analyses combined with Gaussian and Coats-Redfern models to investigate the characteristics and pyrolysis kinetics of sugarcane residue-derived biochars, Journal of Cleaner Production 237
46. Suwanree S, Knijnenburg JTN, Kasemsiri P, Kraithong W, Chindaprasirt P, Jetsrisuparb K (2022) Engineered biochar from sugarcane leaves with slow phosphorus release kinetics, Biomass and Bioenergy 156
47. Han L, Wang Q, Ma Q, Yu C, Luo Z, Cen K (2010) Influence of CaO additives on wheat-straw pyrolysis as determined by TG-FTIR analysis. J Anal Appl Pyrol 88(2):199–206
48. Zhang L, Yao Z, Zhao L, Li Z, Yi W, Kang K, Jia J (2021) Synthesis and characterization of different activated biochar catalysts for removal of biomass pyrolysis tar, Energy 232
49. Wu FC, Tseng RL (2008) High adsorption capacity NaOH-activated carbon for dye removal from aqueous solution. Journal of Hazardous Material 152(3):1256–1267
50. Wang P, Liu X, Yu B, Wu X, Xu J, Dong F, Zheng Y (2020) Characterization of peanut-shell biochar and the mechanisms underlying its sorption for atrazine and nicosulfuron in aqueous solution. Sci Total Environ 702:134767
51. Xiao X, Chen B, Chen Z, Zhu L, Schnoor JL (2018) Insight into multiple and multilevel structures of biochars and their potential environmental applications: a critical review. Environ Sci Technol 52(9):5027–5047
52. Xiao X, Chen B (2017) A direct observation of the fine aromatic clusters and molecular structures of biochars. Environ Sci Technol 51(10):5473–5482

53. Ferrentino R, Ceccato R, Marchetti V, Andreottola G, Fiori L (2020) Sewage sludge hydrochar: an option for removal of methylene blue from wastewater, Applied Sciences 10(10)
54. Jang HM, Kan E (2019) Engineered biochar from agricultural waste for removal of tetracycline in water. Biores Technol 284:437–447
55. Zhang T, Wu X, Fan X, Tsang DCW, Li G, Shen Y (2019) Corn waste valorization to generate activated hydrochar to recover ammonium nitrogen from compost leachate by hydrothermal assisted pretreatment. J Environ Manage 236:108–117
56. Bedia J, Peñas-Garzón M, Gómez-Avilés A, Rodriguez J, Belver C (2018) A review on the synthesis and characterization of biomass-derived carbons for adsorption of emerging contaminants from water, C-Journal of Carbon Research 4(4)
57. Ghanim B, O'Dwyer TF, Leahy JJ, Willquist K, Courtney R, Pembroke JT, Murnane JG (2020) Application of KOH modified seaweed hydrochar as a biosorbent of vanadium from aqueous solution: characterisations, mechanisms and regeneration capacity, Journal of Environmental Chemical Engineering 8(5)
58. Qian WC, Luo XP, Wang X, Guo M, Li B (2018) Removal of methylene blue from aqueous solution by modified bamboo hydrochar. Ecotoxicol Environ Saf 157:300–306
59. Batool S, Idrees M, Al-Wabel MI, Ahmad M, Hina K, Ullah H, Cui L, Hussain Q (2019) Sorption of Cr (III) from aqueous media via naturally functionalized microporous biochar: mechanistic study. Microchem J 144:242–253
60. Qu J, Wang Y, Tian X, Jiang Z, Deng F, Tao Y, Jiang Q, Wang L, Zhang Y (2021) KOH-activated porous biochar with high specific surface area for adsorptive removal of chromium (VI) and naphthalene from water: affecting factors, mechanisms and reusability exploration. J Hazard Mater 401:123292
61. Qi X, Wang H, Zhang L, Xu B, Shi Q, Li F (2020) Removal of Cr (III) from aqueous solution by using bauxite residue (red mud): identification of active components and column tests. Chemosphere 245:125560